Applied Thermal Engineering 288 (2026) 129686

Contents lists available at ScienceDirect

Applied Thermal Engineering

journal homepage: www.elsevier.com/locate/apthermeng

Research Paper

Effect of recycled ceramic particle size on heat transfer and charging dynamics in PCM-based thermal storage systems

Fardin Jafari [a,c,*], Giovanni Semprini [b], Alessandra Bonoli [a], Abhishek Purandare [c], Mina Shahi [c]

[a] Department of Civil, Chemical, Environmental and Materials Engineering, University of Bologna, Italy
[b] Department of Industrial Engineering, University of Bologna, Italy
[c] Department of Thermal and Fluid Engineering, University of Twente, Netherlands

ARTICLE INFO

Keywords:
Thermal energy storage
Phase change materials
Recycled ceramics
Particle size effect
Overheating

ABSTRACT

Heating and cooling account for half of global energy demand, making efficient thermal energy storage (TES) central to decarbonization. Phase change materials (PCMs) can store large amounts of heat, but their low thermal conductivity slows charging and discharging, limiting system performance. To overcome this, metallic fins and foams have been traditionally used to accelerate heat transfer, yet these add complexity, cost, and durability challenges. Here, we explore an alternative pathway: embedding recycled ceramic particles into PCMs to enhance heat transfer while avoiding corrosion and stability issues. Using a lab-scale TES unit, we test composites with different ceramic particle sizes and show that finer particles accelerate charging, enable faster discharge, and suppress overheating compared with coarser particles. This simple modification improves PCM cycling efficiency and reliability.

1. Introduction

Ongoing energy demand has stressed the energy sectors to consume fossil fuels, which has accelerated global warming and climate change. Therefore, governments have invested in renewable energy systems such as wind and solar energy to reduce their reliance on conventional energy sources. However, renewable energies are dispatchable due to their dependency on weather conditions [1,2]. Moreover, surplus energy should be stored properly to prevent the grid from overloading. Thermal energy storage systems play an outstanding role in providing a sustainable energy supply. In addition to renewable energy, thermal storage systems can reduce the energy consumption of various industrial sectors, such as metal manufacturers, through waste heat recovery and management.

Phase change materials (PCMs) are promising options for thermal energy storage due to their high latent heat capacity. However, their relatively low thermal conductivity limits charging and discharging rates, prompting researchers to explore various enhancement strategies [3,4]. Implementing conductive fillers [5] containing graphene [6,7], copper foam [8,9], and carbon fibers [10,11] can improve the heat transfer rate. Compared with other metallic enhancement strategies, fins are widely adopted because they provide predictable heat transfer improvement, can be manufactured with relative ease, and are supported by a large body of experimental and numerical evidence [12,13]. Studies on fin-assisted heat transfer in PCMs have explored a variety of design parameters, including fin thickness [14], number, length, and shape [15,16], as well as the choice of materials [17]. For instance, experiments with aluminum fins and RT27 PCM in a horizontal electric plate setup revealed that increasing fin thickness allows for fewer fins to achieve optimal heat transfer performance [14]. In another vertical electric plate configuration with aluminum fins and lauric acid, adding one fin reduced the total melting time by 18%, while three fins achieved a 37% reduction [17]. Investigations into vertical tubes containing aluminum fins and paraffin wax showed that the inclusion of fins could shorten melting time by as much as 63% [15]. Adjustments to fin shape in paraffin wax-filled vertical tubes led to efficiency gains of about 24% [18], while changes in fin ratio with aluminum fins and organic PCM reduced phase change time by 46% [19]. Comparisons between copper and aluminum fins during the discharging of RT44HC PCM in multi-pass tubes revealed improvements in the average heat transfer rate of 36% and 50%, respectively [20]. Studies combining fin spacing and material selection found that longer fins were more effective in reducing melting time than spacing adjustments alone [21]. Finally, investigations into aluminum fin length with RT55 PCM in vertical tubes demonstrated that optimal configurations could improve melting time by as much as 65%

* Corresponding author at: Department of Civil, Chemical, Environmental and Materials Engineering, University of Bologna, Italy.
E-mail address: fardin.jafari2@unibo.it (F. Jafari).

https://doi.org/10.1016/j.applthermaleng.2025.129686
Received 21 October 2025; Received in revised form 22 December 2025; Accepted 31 December 2025
Available online 5 January 2026
1359-4311/© 2026 The Authors. Published by Elsevier Ltd. This is an open access article under the CC BY license (http://creativecommons.org/licenses/by/4.0/).

Nomenclature

Symbols

cp	Specific heat capacity (kJ/kg·K)
f	Mass fraction
k	Thermal conductivity (W/m·K)
m	Mass (kg)
P	Heater power (W)
Q	Thermal energy (kJ)
SEI	Specific energy input (energy required to melt one kg of composite) (kJ/kg)
T	Temperature (°C)
t	Melting time (s)
V	Volume containing ceramic aggregates and voids (m^3)

Greek

α	Thermal diffusivity (m^2/s)
ΔH_T	Incremental enthalpy at temperature T (kJ/kg)
η	Storage efficiency (%)
θ	Volume fraction
ϕ	Porosity of recycled ceramic aggregates (%)
ρ	Density (kg/m^3)

Subscripts

b	Bulk
con	Container
ef	Effective
f	Final
in	Initial
L	Lower enthalpy boundary
PCM	Phase change material
R	Reference
RC	Recycled ceramic
U	Upper enthalpy boundary
w	Water

[22]. Numerical simulations have also pinpointed an optimal fin length of around 0.2 m for aluminum fins with octadecane under constant wall temperature conditions [16]. Further refinements have examined the role of fin orientation, with stainless steel fins in a vertical electric plate demonstrating that an angle of −15° could accelerate melting by 62.7% [23].

However, building an upscale thermal storage tank with fins raises fabrication costs; the length, thickness, space, and materials should be optimized. Furthermore, fins have poor resistance to the corrosive effects of PCMs, which degrade their performance over time [24–27]. Therefore, incorporating recycled ceramic (RC) aggregate into PCMs offers a sustainable and efficient approach to enhancing thermal energy storage systems [28]. Recycled ceramics, derived from construction and demolition waste, possess favorable thermal properties such as high effective thermal diffusivity and thermal stability, which can improve the heat transfer performance of PCM. Their porous structure also facilitates better PCM encapsulation and retention, reducing the risk of leakage during phase transitions. Furthermore, utilizing recycled ceramics aligns with circular economy principles by reducing landfill waste and lowering the environmental impact of material sourcing. The integration of recycled ceramic aggregates with PCM in varying particle sizes provides a promising strategy for optimizing thermal response and energy efficiency in heat storage applications.

The primary novelty of this study lies in combining recycled ceramic particles with PCM for latent heat thermal storage applications, as such compounds have mainly been used in producing building materials like ceiling and roofing tiles [29,30].

This work specifically investigates the influence of particle size on melting time and temperature distribution within the storage medium. Another objective of this study is to monitor the overheating issue, which is significantly intensified by natural convection. Although natural convection enhances heat transfer in phase change materials (PCMs), it also causes higher temperature accumulation at the top of the thermal storage enclosure, thereby reducing the cycle life of both the PCM and the container. Overheating can occur during rapid charging cycles aimed at achieving optimum efficiency when using non-dispatchable sources such as photovoltaic (PV) panels. Moreover, large temperature gradients complicate the management of outlet energy in hot water distribution systems.

In addition, recycled ceramics also support sustainability and the circular economy, being nearly carbon-neutral and widely available at low cost, whereas PCMs typically emit about 4 kg CO_2 per kilogram [31,32] and cost around 15€ per kilogram [33]. By incorporating recycled ceramic particles, heat transfer can be improved, temperature distribution can be more uniform, and system design becomes more reliable. These advantages make the composite particularly suitable for large-scale applications requiring rapid charging.

2. Methods and materials

2.1. Material preparation and thermal property assessment

In this study, RC obtained from construction and demolition waste was utilized as a filler material in latent heat thermal energy storage systems. The waste ceramic was crushed and classified into three particle size categories using sieving baskets: A1 (0.18–0.6 mm), A2 (0.9–1.4 mm), and A3 (1.7–2.36 mm), following the procedure described by Xu et al. [24]. The RC particles were thoroughly washed and oven-dried at 105 °C for three days to eliminate dust and impurities that could influence experimental results [34]. Subsequently, each RC category was placed into a Graduated Cylinder Glass up to a volume of 50 ml (± 0.5 ml) to determine bulk density and porosity. The bulk density (ρ_b) of the RC aggregates and porosity (ϕ) of the packed bed were calculated using Eqs. (1) and (2) [35–37], respectively, and are presented in Fig. 1:

$$\rho_b = \frac{m_{RC}}{V_t} \tag{1}$$

where m_{RC} is the mass of the recycled ceramic aggregates, and V_t is the total volume, containing both ceramic aggregates and voids. The porosity of the packed bed (ϕ) is described as a percentage and can be

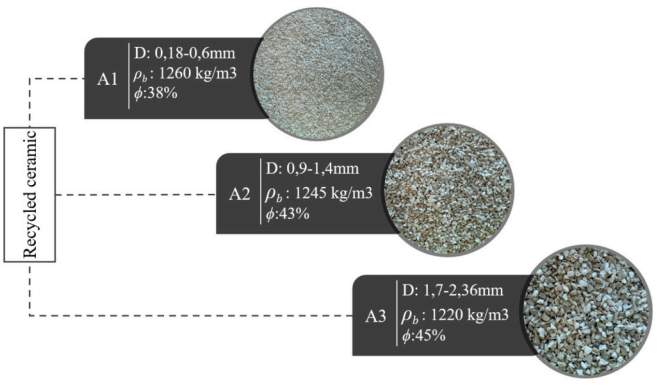

Fig. 1. Porosity and bulk density of recycled ceramics aggregates based on their categorized size.

determined as Eq. (2):

$$\phi = \frac{V_v}{V_t} \times 100\% \quad (2)$$

The term V_v denotes the void volume, while V_t refers to the total volume.

To prepare the RC–PCM composites, each category of recycled ceramic was mixed with pure PCM in a fixed mass ratio of 300 g ceramic to 100 g PCM, filling almost the porosity of ceramic particles, which is compared with a 198 g only PCM sample donated by R-PCM. Achieving a homogeneous mixture was essential; therefore, both the RC and PCM were preheated to 60 °C, exceeding the PCM's melting point (specified in Table 1). The heated materials were then sequentially poured into the storage container. Continuous heating was applied via a central heating element to prevent partial solidification.

The specific heat capacity of the recycled ceramic aggregates was characterized using a Hot Disk TPS 100 instrument [38]. Additionally, thermal conductivity was evaluated using the heat flow meter method, which determines steady-state thermal conductivity for materials with λ < 5 (W/mK) [39–42]. This method complies with ISO 9301 standards [39–42]. The apparatus was designed following ISO 8301 and employs two heat flow meters in a single-specimen symmetrical configuration, with a helical counter-flow path supplying the hot and cold plates through a circulating liquid (Fig. 2). Plate temperatures are controlled using thermostatic baths ranging from −15 to +90 °C. The working surfaces are made of copper and finished to a flatness within 0.02%. An IR thermo-camera verified temperature uniformity, which should not exceed 1% of the temperature difference across the specimen [43].

RT44HC was selected as the PCM due to its frequent application in latent heat thermal energy storage systems, as reported in previous studies [44–47]. The thermal and physical properties of the PCM, ceramic aggregates, are summarized in Table 1.

The effective thermal diffusivity (α_{eff}) characterizes the rate at which heat propagates through a material and is particularly important for composites containing phase change materials (PCM), where transient thermal response governs performance in thermal energy storage applications. In a composite of recycled ceramic and PCM, α_{eff} can be estimated using:

$$\alpha_{eff} = \frac{K_{eff}}{\rho_{eff} \times cp_{eff}} \quad (3)$$

where k_{eff} is the effective thermal conductivity, ρ_{eff} is the effective density, and $c_{p,\text{eff}}$is the effective specific heat capacity of the composite.

The effective thermal conductivity of the PCM-filled ceramic was estimated using the Maxwell–Eucken model, suitable for composites with inclusions dispersed in a continuous matrix, 4–6:

$$K_{eff} = K_s \frac{K_i + 2K_s - 2\theta(K_s - K_i)}{K_i + 2K_s - \theta(K_s - K_i)} \quad (4)$$

where k_s and k_{PCM} are the thermal conductivities of the ceramic skeleton and PCM, respectively, and θ is the PCM volume fraction. For the present system, the sample masses are 300 g of ceramic and 100 g PCM, giving a PCM fraction of $\theta \approx 0.25$. With $k_s = 2$ W/(m.K) and the effective thermal conductivity is $k_{eff} \approx 1.49$ W/(m.K), which lies reasonably between the conductivities of the two components.

The effective density and specific heat were calculated using the volume-weighted averaging (Voigt) model, assuming uniform distribution and thermal equilibrium:

$$\rho_{eff} = (1-\theta)\rho_s + \theta\rho_{PCM} \quad (5)$$

$$cp_{eff} = (1-\theta)cp_s + \theta cp_{PCM} \quad (6)$$

where ρ_s and $c_{p,s}$ are the density and specific heat of the finest ceramic, and ρ_{PCM} and $c_{p,PCM}$ are those of the PCM. Considering $\rho_s = 1260$ kg/m^3 and $c_{p,s} = 0.75$ kJ/kg.K for the ceramic, and $\rho_{PCM} = 700$ kg/l and $c_{p,PCM} = 2.0$ kJ/kg. K for the PCM, the effective properties of the composite are calculated as $\rho_{eff} = 1180$ kg/m^3 and $c_{p,eff} = 1.06$ kJ/kg.K. Substituting these values into the thermal diffusivity definition for RC-PCM matrix gives:

$$\alpha_{eff} = \frac{K_{eff}}{\rho_{eff} \times cp_{eff}} = \frac{1.49}{1180 \times 1060} \approx 1.19 \times 10^{-6}\ m^2 \Big/ s \quad (7)$$

This value lies between the thermal diffusivities of the pure PCM ($\alpha_{PCM} \approx 1.43 \times 10^{-7}$ [m^2/s]) and the ceramic, reflecting the influence of the low-conductivity PCM inclusions, while the continuous ceramic matrix enhances heat transfer. Thus, incorporating the ceramic skeleton significantly increases the effective thermal diffusivity, thereby improving the heat transfer rate of the composite system.

Table 1
Thermophysical properties of PCM (RT-44HC) and all three types of RC aggregates used in this work.

Property	PCM	RC (A1)	RC (A2)	RC (A3)
Melting range [°C]	41–44	–	–	–
Solidification range [°C]	44–40	–	–	–
Latent heat of fusion [kJ/kg]	250	–	–	–
Specific heat capacity [kJ/kg.K]	2	0.75	0.7	0.6
Density in solid state [kg/m^3]	800	1260	1245	1220
Density in liquid state [kg/m^3]	700	–	–	–
Thermal conductivity [W/(m.K)]	0.2	0.21	0.18	0.14
Volume expansion [%]	12.5	–	–	–

2.2. Experimental setup

In this study, a small-scale latent heat thermal energy storage unit was developed, consisting of three main components: the storage medium, a cylindrical container, and a heat source. The storage medium comprises a composite of recycled ceramic and the commercially available RT44HC, supplied by Rubitherm GmbH. The cylindrical container is fabricated from a 5 mm thick PA200 plastic, with internal dimensions of 60 mm in diameter and 95 mm in height, with a mass of 140 g. To minimize heat losses, the container is insulated with a 20 mm thick ceramic wool layer around its lateral surface.

An electric heating element, 6 mm in diameter and rated at a maximum power of 305 W, is centrally positioned within the container and powered by an external power generator. Two T-type thermocouple arrays (accuracy ±0.1 °C) are installed on the surface of the heating element to monitor the vertical temperature profile. Data acquisition is performed using a cDAQ system (National Instruments), with real-time data transfer to a computer for analysis. The experimental setup, including the enclosure and thermocouple arrangement, is illustrated in Fig. 3.

2.3. Data acquisition and theoretical calculation

In this study, pure PCM and RC-PCM compounds are evaluated using an identical data acquisition procedure under two constant input powers: 5.3 W and 6 W. The thermal performance of the storage medium is assessed by monitoring the temperatures. Specifically, when the lowest temperature of the thermocouples increased from 20 °C (ambient room temperature) up to 51 °C [45], which corresponds to the upper boundary of the PCM's enthalpy range. Under these conditions, it is assumed that the PCM is fully molten.

The thermal energy storage can be calculated based on the temperature change of the storage medium. Regarding the PCM thermal behavior corresponding to the temperature change, it undergoes a phase transition while the temperature is between 36 °C and 51 °C, during which it absorbs both sensible and latent heat (enthalpy), accumulating 260 kJ/kg [33]. However, the PCM stores sensible heat below and above the mentioned temperature ranges. Conversely, recycled ceramic is

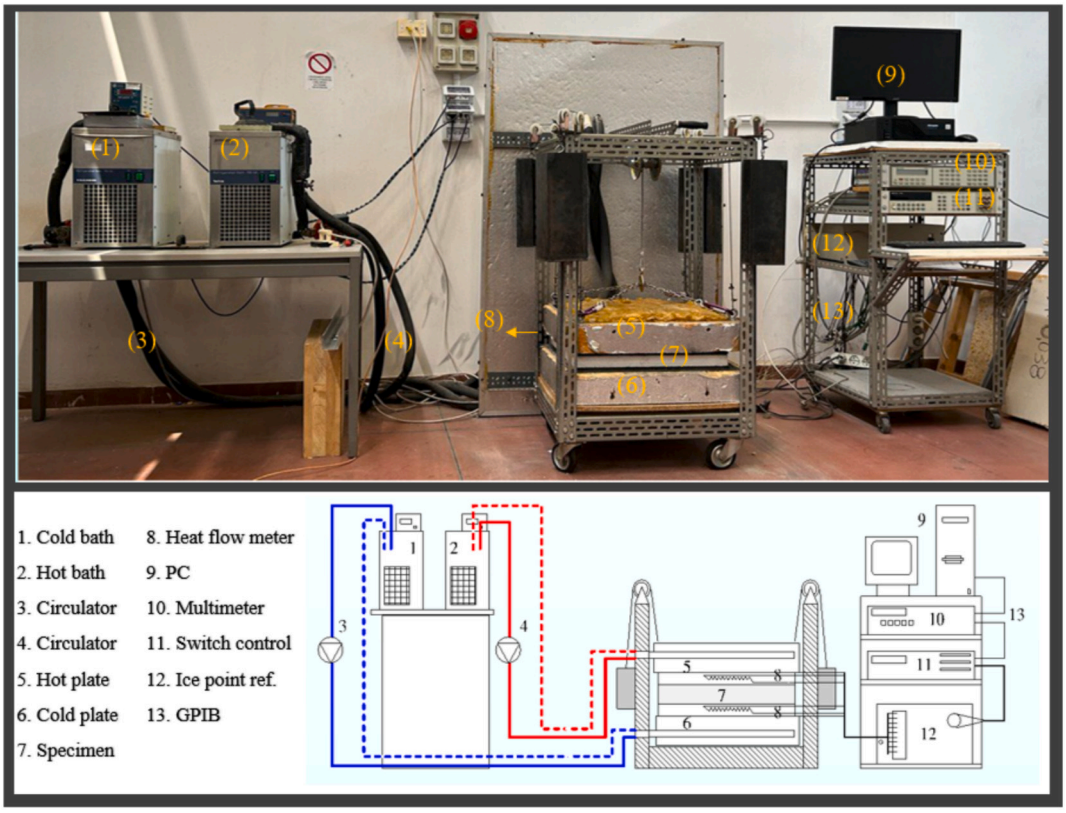

Fig. 2. The heat flow meter apparatus used for thermal conductivity measurements, highlighting the main components and configuration.

considered for its sensible heat.

Due to temperature variations within the storage container, the theoretical thermal-energy calculation uses the average temperature of the storage medium [48], measured at three vertical positions: top (T1), middle (T2), and bottom (T3). In addition to the storage medium, the thermal absorption of the container itself was included in the energy calculation. The energy stored by the reference PCM (R-PCM) Specimen can be estimated using the following equation:

$$Q_{R-PCM} = Q_{con} + Q_{PCM} \tag{8}$$

$$Q_{con} = m_{con} cp_{con} \left(T_f - T_{in}\right) \tag{9}$$

$$Q_{PCM} = Q_{s,PCM} + Q_{H,PCM} + Q_{l,PCM} \tag{10}$$

$$Q_{s,PCM} = m_{PCM} cp_{PCM} \left(T_{H,L} - T_{in}\right) \tag{11}$$

$$Q_{H,PCM} = m_{PCM} \sum_{T=T_L}^{T_U} \Delta H_T \tag{12}$$

$$Q_{l,PCM} = m_{PCM} cp_{PCM} \left(T_f - T_{H,U}\right) \tag{13}$$

where Q_{R-PCM} represents the total thermal energy stored by the PCM-based unit, which comprises the heat absorbed by the container (Q_{con}) and that absorbed by the phase change material (Q_{PCM}). m *and* c_p expressed the mass and specific heat capacity of the materials, calculated in kg and kJ·kg^{-1}·K^{-1}, respectively. The initial temperature of the system (T_{in}) is 20 °C, while T_f is the final temperature, which is variable. The lower and upper limits of the PCM enthalpy range are described by $T_{H,L}$ = 36 °C and $T_{H,U}$ = 51 °C, respectively. The term ΔH_T (kJ/kg^{-1}) denotes the incremental enthalpy change of the PCM during the melting process. The quantities $Q_{s,PCM}$, $Q_{H,PCM}$, and $Q_{l,PCM}$ correspond to the sensible heat stored in the solid phase, the enthalpy heat absorbed during the phase transition, and the sensible heat stored in the liquid phase, respectively, all expressed in joules (J).

The stored energy by RC-PCM compounds ($Q_{RC\text{-}PCM}$) can be calculated with Eqs. (14) and (15):

$$Q_{RC-PCM} = Q_{con} + Q_{PCM} + Q_{cer} \tag{14}$$

$$Q_{cer} = m_{cer} c_{p,cer} \left(T_f - T_{in}\right) \tag{15}$$

where, Q_{con}, Q_{PCM} and Q_{cer} denote the energy stored by the container, phase change material (PCM), and ceramic, respectively. The symbols m_{cer} and $c_{p,cer}$ represent the mass and specific heat capacity of the ceramic, respectively. The stored energy of the container and PCM can be determined using Eqs. (9)–(13).

The storage efficiency was determined as the ratio of the stored thermal energy to the effective input energy, considering the heat losses occurring during the charging process. This formulation is appropriate since only the charging phase was analyzed in the present work, without a discharging cycle. The efficiency (η) is expressed as:

$$\eta_{R-PCM} = \frac{Q_{R-PCM}}{Q_{e,in}} \times 100\% \tag{16}$$

$$\eta_{RC-PCM} = \frac{Q_{RC-PCM}}{Q_{e,in}} \times 100\% \tag{17}$$

where $\eta_{R\text{-}PCM}$ and $\eta_{RC\text{-}PCM}$ represent the storage efficiencies of the reference PCM and the recycled ceramic–PCM composite, respectively, expressed in percentage. $Q_{e,in}$ denotes the total electrical input energy supplied to the system.

The data obtained from the experimental tests were used to calculate the Specific Energy Input (SEI) for each scenario. The indicator SEI_{PCM} represents the total energy required to completely melt the PCM, normalized by the PCM mass and expressed in kJ/kg [44]. These parameters are useful for comparing composite samples containing different PCM fractions. The SEI_{PCM} is calculated using Eq. (18): [47].

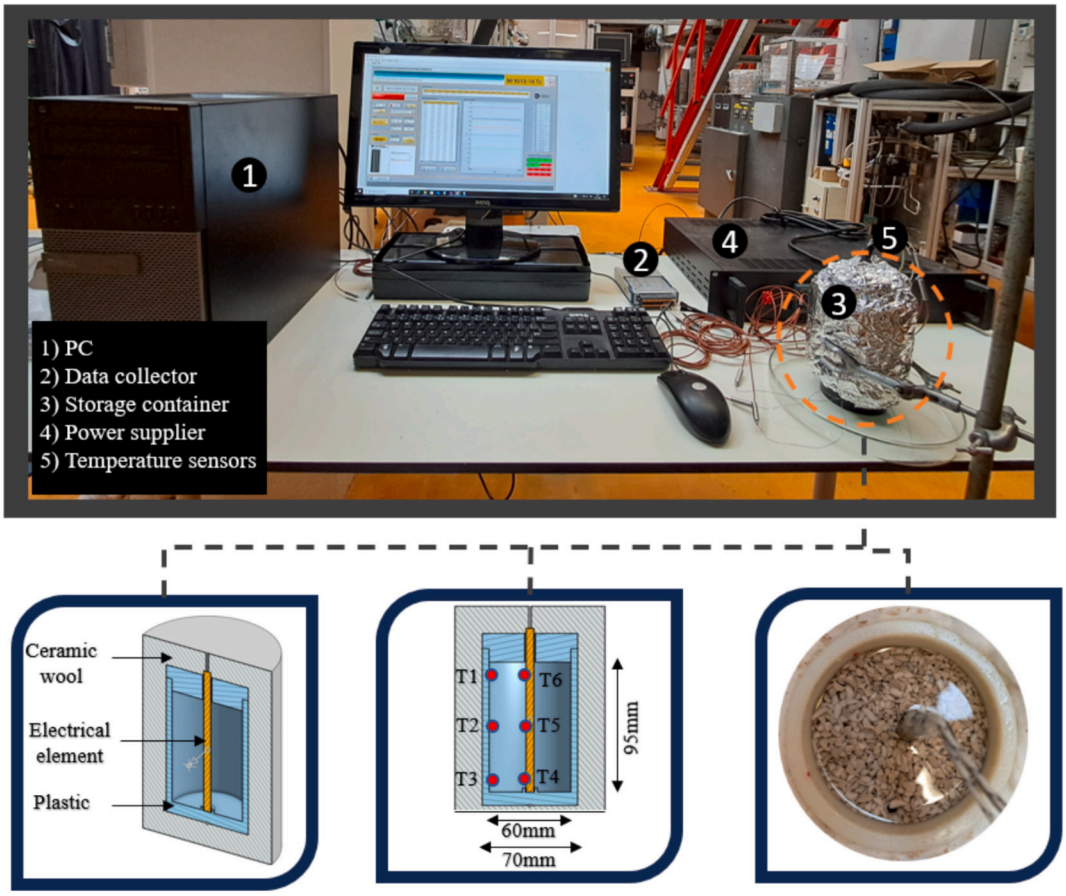

Fig. 3. Experimental setup showing container dimensions, cross-section, and RC–PCM composite.

$$SEI_{PCM} = \frac{Q_{PCM}}{m_{PCM}} \tag{18}$$

where Q_{PCM} is the total energy absorbed by the PCM during melting (kJ), referring to Eq. (10)–(13).

In this study, overheating was quantified based on the duration during which the top-side PCM temperature exceeded the maximum operating temperature of 70 °C [33], relative to the total time required for complete melting of the PCM within the storage container. The total melting time ($t_{tot,melt}$) was defined as the interval from when the lowest PCM temperature reached 51 °C until the entire PCM had fully melted. The overheating percentage was then calculated as:

$$Overheating = \frac{t_{tot,melt} - t_{overheat}}{t_{tot,melt}} \times 100\% \tag{19}$$

2.4. Uncertainty analysis

To evaluate the reliability of the experimental measurements of thermal energy input during PCM melting, the combined measurement uncertainty was analyzed. The total thermal energy input Q during the melting process is calculated as:

$$Q = P \times t \tag{20}$$

The combined uncertainty in Q must then be quantified by propagating the individual uncertainties associated with P and t. Assuming these variables are independent, the combined relative uncertainty is given by the root-sum-square of their individual relative uncertainties [49,50]:

$$\frac{u(Q)}{Q} = \sqrt{\left(\frac{u(P)}{P}\right)^2 + \left(\frac{u(t)}{t}\right)^2} \tag{21}$$

here $u(Q)$, $u(P)$, and $u(t)$ represent the absolute uncertainties in Q, P, and t, respectively. The power P is measured with an uncertainty derived from the voltage and current measurements, while the melting time t is obtained from temperature-based time recordings. This method of uncertainty propagation follows the internationally recognized Guide to the Expression of Uncertainty in Measurement (GUM) framework [50] and has been applied in recent experimental studies involving phase change materials and thermal energy storage systems [51]. Using Eqs. (20) and (21), the uncertainty associated with the thermal power was calculated as 1.2%.

3. Results and discussion

3.1. Charging temperature distribution

Fig. 5 presents the temperature profiles (T1, T2 and T3) of the storage media within the latent heat enclosure during the charging cycle for the three categories of RC-PCM (a, b, c) and R-PCM (d), with an input power of 5.7 W. Sensors T4, T5, and T6 were mounted directly on the heater surface, where they measured the heater's temperature rather than the PCM. Their readings reflect local conductive heating and not the bulk thermal behavior of the storage medium. To avoid misinterpretation of the PCM temperature profiles, these sensors were excluded, as their elevated values indicate only the expected strong conduction near the heater rather than the PCM's actual thermal response. The enthalpy range and the overheating zone are indicated in yellow and red, respectively. The peak melting temperature of RT-44HC (43 °C)

[33] is marked by the horizontal dashed lines in the figures. Furthermore, the mean temperature (green line) represents the average of sensors T1, T2, and T3.

As shown in Fig. 5, all storage samples exhibited a significant trend change upon reaching 51 °C. During the charging process, the R-PCM cylindrical storage unit exhibits a vertical temperature gradient, with higher values at the top. This can be attributed to buoyancy-driven natural convection, as the PCM near the centrally located heater melts, the lighter liquid rises while the cooler, denser PCM settles at the bottom [52,53], referring to Fig. 4. This circulation enhances heat transfer in the upper region, resulting in higher temperatures recorded by the top thermocouples. The vertical orientation of the cylinder further promotes this convective flow and thermal stratification.

Comparing the temperature profiles of RC-PCM (a, b, c) with R-PCM revealed that RC-PCM compounds significantly reduce thermal gradient. Compound A1 demonstrated a minimum temperature gradient of 21 °C over the charging cycle, whereas the PCM-based unit recorded a temperature difference of 48 °C, effectively doubling the stratification. This thermal gradient leads the top region of the thermal storage medium into the overheating zone. Under these conditions, the top of the PCM remained in the overheating zone for 63% of the total charging time, which was 14%, 22%, and 43% higher than for A3, A2, and A1, respectively.

Regarding the melting time, the results indicated that RC-PCM compounds enable faster charging than the PCM-based unit due to the reduced PCM mass in the matrix. Among the RC-PCM compounds, A1 exhibited the fastest charging, completing the cycle within 200 min, which decreased the melting time compared to A2 and A3 by 2 min and 10 min, respectively. In contrast, the R-PCM unit exhibited the longest charging cycle, lasting 302 min.

As shown in Fig. 6, increasing the input power from 5.7 W to 6 W significantly affects the temperature distribution within the storage mediums. Comparing the two input powers reveals that a 5% increase in power reduced the melting time by approximately 22% across all samples, with A1 melting in 156 min, A2 in 158 min, A3 in 167 min, and the PCM unit in 240 min. However, this increase in input power also intensified thermal gradient and the overheating effect. Sample A1, with finer particles, exhibited the smallest increase in thermal stratification, rising only 2 °C from ΔT = 21 °C to ΔT = 23 °C. In contrast, the R-PCM unit showed a much larger increase of 11 °C, reaching 59 °C. The overheating results followed a similar trend: finer particles in A1 led to a modest increase in overheating of 4%, reaching 9%, whereas A2, A3, and the PCM unit experienced larger increases of 22%, 35%, and 69%, respectively. These results indicate that finer RC particles mitigate the negative effects of higher input power on temperature gradient and overheating compared to coarser particles or pure PCM.

The observed results show a clear correlation between the particle size of the recycled ceramic (RC) in the RC-PCM composites and both thermal gradient and melting time. Due to its higher expected thermal diffusivity value, A1 has a faster heat propagation throughout the composite, which, combined with the smaller particle size and uniform distribution within the PCM matrix, creates an efficient thermal network. This enhanced heat transfer reduces vertical temperature gradients and natural convection, resulting in the lowest thermal gradient in 5.7 W (ΔT = 21 °C) and 6 W (ΔT = 23 °C), and accelerates melting, allowing A1 to complete the charging cycle faster than the other composites. In contrast, medium (A2) and coarse (A3) particles have lower thermal diffusivity, creating larger void spaces, which allow heat to rise more rapidly through natural convection. The less uniform dispersion, which limits heat propagation, causes localized overheating near the top, increases thermal stratification, and prolongs melting. The pure PCM unit exhibits the highest thermal gradient and the longest melting time because heat transfer relies solely on conduction through the solid PCM and buoyancy-driven convection in the liquid phase, which is less efficient than the combined conduction and diffusion network provided by RC particles. Overall, the higher thermal diffusivity of finer RC particles in A1 improves heat distribution, minimizes thermal stratification, and shortens melting time, whereas coarser particles or pure PCM result in stronger vertical temperature gradients and slower charging.

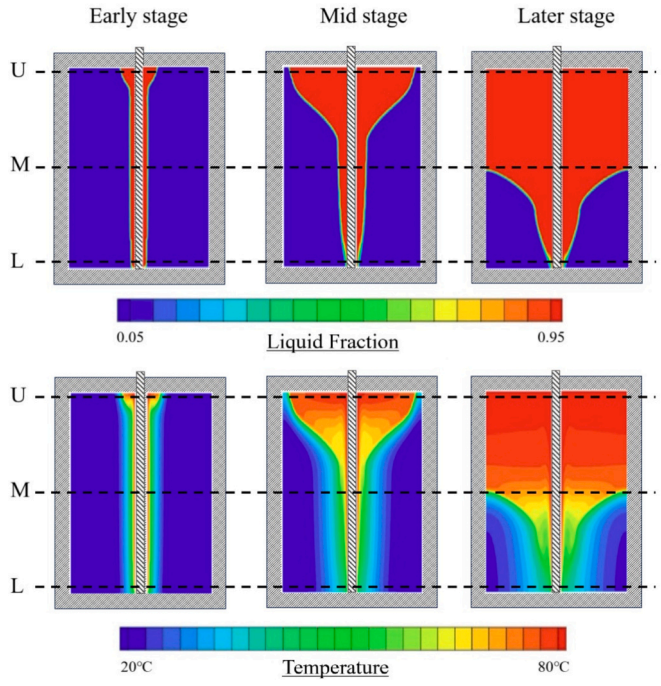

Fig. 4. Evolution of the liquid fraction and temperature distribution of the PCM in a cylindrical enclosure with a centrally positioned heater during early, mid, and later stages of melting [52]. The symbols U, M, and L represent the upper, middle, and lower regions of the container, respectively.

3.2. Thermal storage performance

Fig. 7 illustrates the storage performance of the tested thermal media. The R-PCM unit stored approximately 80 kJ of energy at an input power of 5.7 W during a charging cycle, about 60% higher than the RC-PCM composites. This difference is primarily due to the higher PCM mass fraction: R-PCM contains 198 g of PCM, nearly double the 100 g in RC-PCM. The larger PCM mass provides more latent material to absorb heat during phase change, resulting in greater total energy storage under the same heating conditions. An evaluation of the heat loss indicator showed that approximately 25% of the total input heat was lost at 5.7 W during charging, resulting in overall storage efficiencies below 80% due to the longer charging process. At 6 W, the heat loss slightly increased because of higher temperature gradients, reducing the storage efficiency by a few percentage points. Nevertheless, the R-PCM exhibited higher efficiency (~76%) compared to the RC-PCM composites (70–73%). These results indicate that while increasing input power accelerates charging, it also slightly increases heat loss, which must be considered when optimizing thermal storage performance.

When the input power increased to 6 W, the amount of stored energy did not change significantly. However, the higher input power substantially reduced heat losses by approximately 15% due to reducing melting time, resulting in values of 9% for A1, 10% for A2, 13% for A3, and 5% for R-PCM. This reduction in heat loss enhanced the thermal storage efficiency of all samples during the charging cycles. The highest efficiency was recorded for PCM at 95%, followed by A1 (90.8%), A2 (90.4%), and A3 (87.4%).

The results in Fig. 7 also indicate a correlation between input power, thermal storage efficiency, and overheating behavior. Lower input power extends the charging duration, allowing for more uniform heat

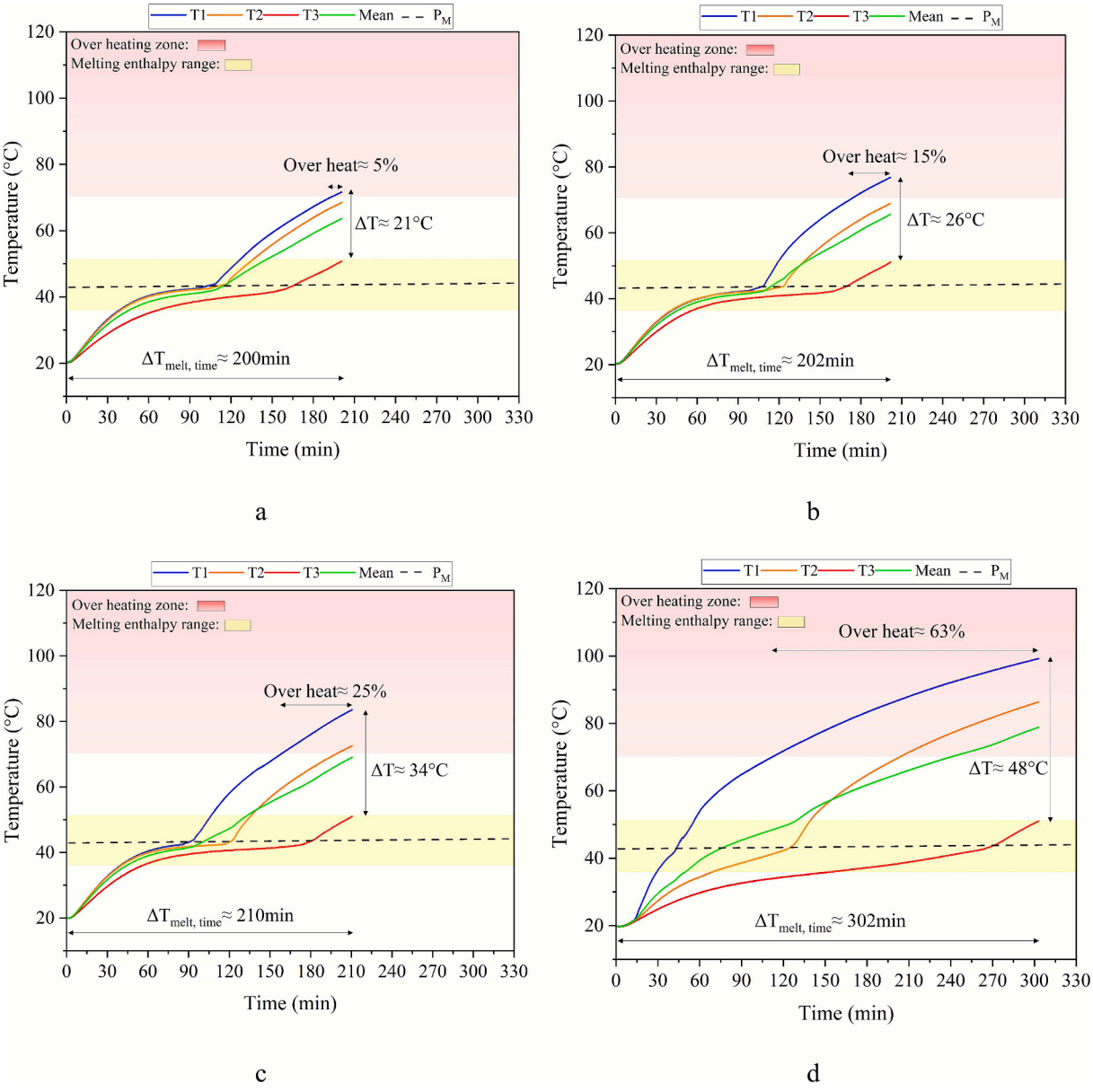

Fig. 5. Temperature profiles of the thermal storage medium during the charging cycle over time under a constant input power of 5.7 W: (a) A1 [0.18–0.6 mm], (b) A2 [0.9–1.4 mm], (c) A3 [1.7–2.36 mm], and (d) R-PCM.

distribution within the storage medium and mitigating localized overheating. However, prolonged charging time increases overall heat loss, thereby reducing efficiency. Conversely, applying a higher input power (6 W) shortens the melting time and minimizes heat loss, leading to improved storage efficiency in the thermal units. The combination of finer RC particles (a1) and 6 W input power yielded the most efficient and stable performance, as the improved diffusivity enabled uniform heat distribution while preventing the overheating and stratification observed with coarse particles or elevated power levels.

3.3. Specific energy input

Fig. 8 presents the variation in specific energy input per unit mass (SEI_{PCM}) for the recycled ceramic-PCM composite configurations (A1, A2, A3), the pure PCM, and the system reported by Fadl et al. [48] In their study, Fadl et al. developed a latent heat thermal energy storage system (LHTESS) consisting of a shell integrated with a horizontally oriented multi-tube heat exchanger to accelerate the charging and discharging processes. Instead of incorporating fins, they employed extended heat exchanger tubes, using the same PCM (RT-44HC) and a target operating temperature of 51 °C.

As shown in the figure, the reference PCM required approximately 353 kJ to completely melt 1 kg of material. The use of RC-PCM composites reduced the specific energy input, with configuration A1 showing a decrease of about 10%, reaching 318.44 kJ/kg. Similarly, configurations A2 and A3 exhibited reductions of approximately 8% and 6%, respectively. Fadl et al. reported a specific energy input of 333.4 kJ/kg, which is about 4% higher than that of configuration A1. This reduction indicates that the RC-PCM composites enhance charging performance by facilitating faster and more efficient heat absorption due to improved thermal diffusivity and more uniform heat distribution. In contrast, Fadl et al. used a longer heat exchanger to increase heat transfer, which accounts for their higher specific energy input.

The reduced specific energy input observed for finer ceramic particles is attributed to their larger surface-area-to-volume ratio, which enhances the effective thermal diffusivity of the composite. This results

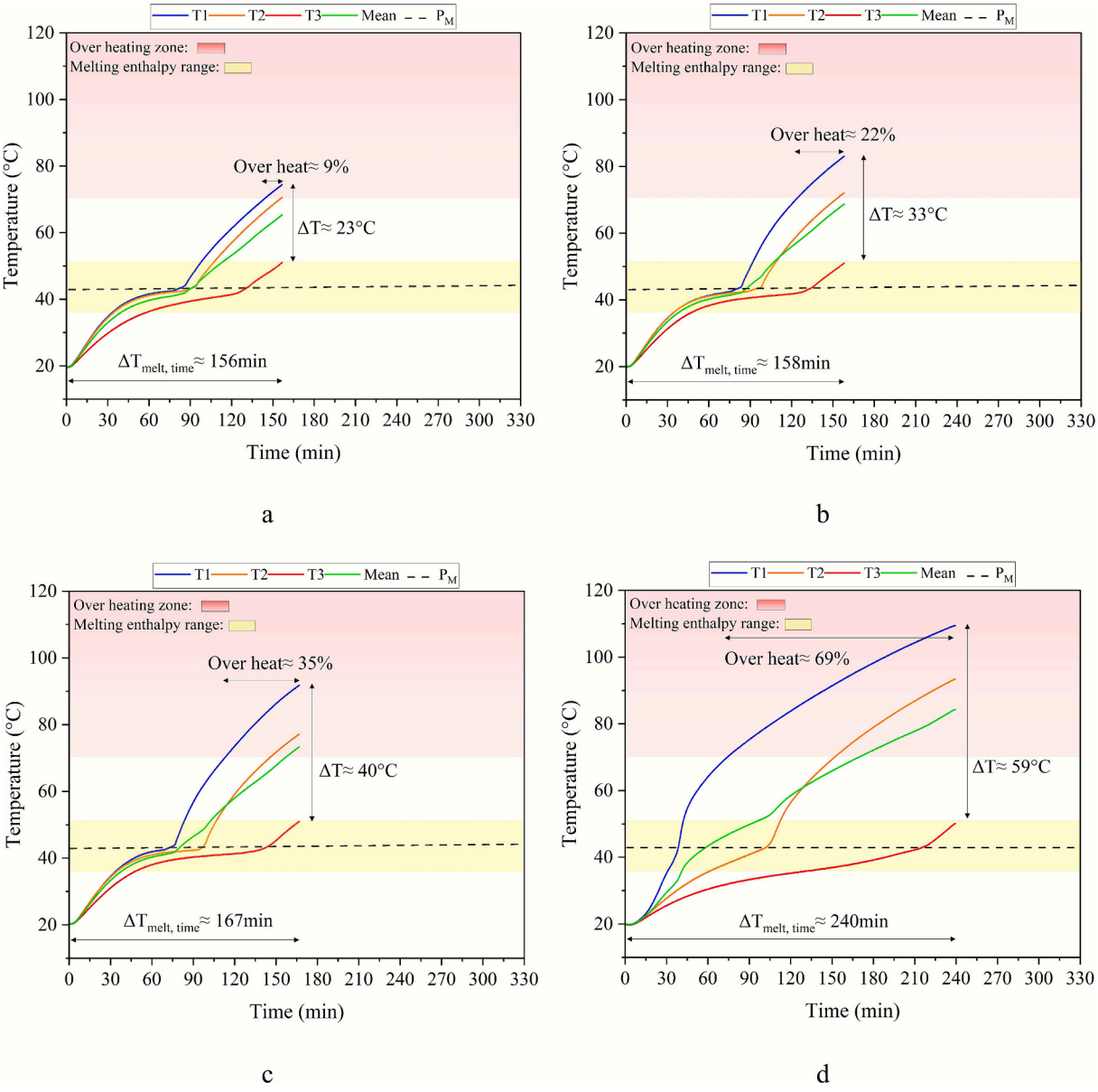

Fig. 6. Temperature profiles of the thermal storage medium during the charging cycle over time under a constant input power of 6 W: (a) A1 [0.18–0.6 mm], (b) A2 [0.9–1.4 mm], (c) A3 [1.7–2.36 mm], and (d) R-PCM.

in more uniform and efficient heat propagation within the PCM, enabling faster charging and lowering the energy required per unit mass.

4. Conclusion

This study investigates the effect of recycled ceramic particle size on the thermal performance of a phase change material (RT44HC) in a latent heat thermal energy storage system. Recycled ceramic particles were categorized into three size ranges A1 (0.18–0.6 mm), A2 (0.9–1.4 mm), and A3 (1.7–2.36 mm), and incorporated into the PCM to form composite samples (RC-PCMs) and compared with a PCM-based storage unit. Thermal behavior was characterized in a cylindrical enclosure with a central electrical heater operating at constant power inputs of 5.7 W and 6 W.

The thermal performance of RC-PCM composites strongly depends on the size of recycled ceramic (RC) particles. Finer particles (A1) exhibited higher thermal diffusivity, enabling faster heat propagation, more uniform temperature distribution, and reduced vertical gradients. This resulted in the lowest vertical temperature gradient ($\Delta T = 21$ °C at 5.7 W, $\Delta T = 23$ °C at 6 W), the shortest melting time, and minimal overheating compared to coarser particles (A2, A3) and pure PCM. Medium and coarse particles showed slower heat transfer, higher stratification, and localized overheating. Meanwhile, pure PCM relied solely on conduction and convection, resulting in the slowest charging cycle and a higher overheating rate. Increasing input power from 5.7 W to 6 W accelerated melting and reduced heat loss. Overall**, a balanced input power combined with finer ceramic particles** provides the most efficient, stable, and reliable configuration for latent heat thermal energy storage systems.

Future research should focus on evaluating long-term cycling stability, assessing the effects of particle shape and distribution, optimizing the combination of input power and RC particle characteristics, characterizing matrix thermal properties (e.g., specific heat and thermal conductivity), performing dimensionless analyses (e.g., Fourier and Stefan numbers) to generalize the findings, and evaluating the cost implications of large-scale sourcing, processing, and integration of recycled ceramics.

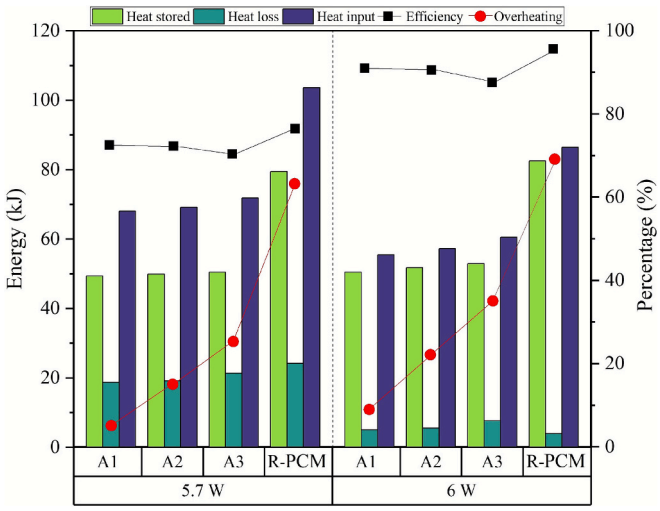

Fig. 7. Comparison of heat input, heat stored, heat loss (kJ), storage efficiency (%), and overheating ratio (%) for the R-PCM and RC-PCM composite samples (A1, A2, A3) under constant input power of 5.7 W and 6 W.

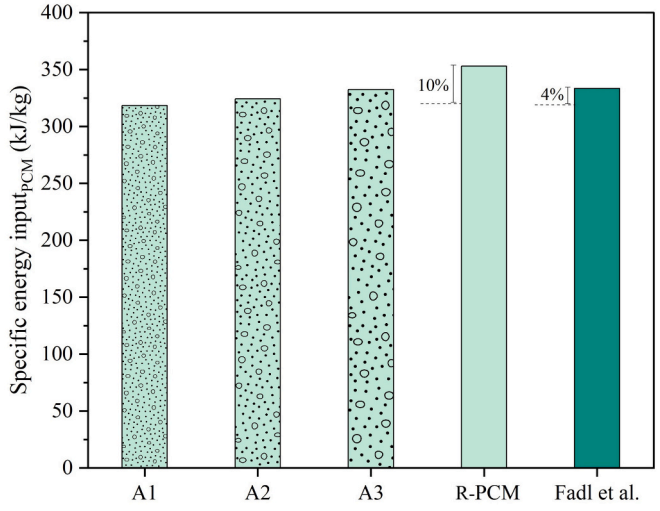

Fig. 8. Specific energy input per PCM mass (SEI_{PCM}) for R-PCM and ceramic-PCM composites (A1, A2, and A3) and reference data from Fadl et al. [48].

CRediT authorship contribution statement

Fardin Jafari: Writing – original draft, Visualization, Validation, Project administration, Methodology, Investigation, Formal analysis, Data curation, Conceptualization, Writing – review & editing. **Giovanni Semprini:** Resources, Methodology, Investigation. **Alessandra Bonoli:** Supervision, Resources, Methodology, Investigation. **Abhishek Purandare:** Writing – review & editing, Validation, Supervision, Investigation, Formal analysis. **Mina Shahi:** Writing – review & editing, Supervision, Resources, Methodology, Investigation, Funding acquisition, Formal analysis.

Declaration of competing interest

The authors declare that they have no known competing financial interests or personal relationships that could have appeared to influence the work reported in this paper.

Acknowledgments

The authors would like to express their sincere gratitude to Henk Jan Moed, Bas Overtoom, and Aastha Arya from the Department of Thermal and Fluid Engineering, University of Twente, for their valuable technical and research assistance. The authors also wish to thank Maurizio Chendi from the Department of Industrial Engineering, University of Bologna, for his support and collaboration during the experimental activities.

Data availability

Data will be made available on request.

References

[1] J. Lee, Y.T. Yoon, G.-J. Lee, Renewable energy sources: from non-dispatchable to dispatchable, and their application for power system carbon neutrality considering system reliability, J. Electr. Eng. Technol. 19 (2024) 2015–2028, https://doi.org/10.1007/s42835-023-01669-8.
[2] F. Gökgöz, Ö. Yücel, Merit-order of dispatchable and variable renewable energy sources in Turkey's day-ahead electricity market, Util. Policy 88 (2024) 101758, https://doi.org/10.1016/j.jup.2024.101758.
[3] X. Hu, P. Chen, X. Guo, X. Zhang, Comparative studies on the thermal performance of novel PCM-based heat sinks using 3D-printed thermal conductivity enhancers, Int. Commun. Heat and Mass Transf. 162 (2025) 108613.
[4] B. Çiçek, A numerical comparison of the thermal performances of nano-PCM heat sinks with Fe3O4, MgO, ZnO and xGNP nanoparticles: Key role of increased thermal conductivity, Thermal Science and Engineering Progress 63 (2025) 103712, https://doi.org/10.1016/J.TSEP.2025.103712.
[5] A. Sathishkumar, P. Sundaram, S.P. Ranga, P.G. Kumar, M. Cheralathan, R. Velraj, Role of *aloe vera* based nanofluids for cool thermal energy storage system: A comparative study, J. Energy Storage 90 (2024) 111710, https://doi.org/10.1016/J.EST.2024.111710.
[6] N.K.G. Ranga, P. Verma, S.K. Gugulothu, P. Gandhi, Thermal performance optimization of PCM Systems using graphene nanoparticles and advanced fin geometries under variable heat input conditions, Energy Storage 7 (2025) e70238.
[7] P. Vigneshwaran, S. Shaik, S. Arulmani, M. Arıcı, T. Alam, A.H. Shaik, Incorporation of graphene nanoplatelets with organic phase change materials–Studies on thermal conductivity enhancement, and thermal and chemical stability, Int. J. Thermofluids 20 (2023) 100456.
[8] A. Kotb, S. Wang, Enhanced thermal storage performance with non-linear porosity distribution in copper foam-PCM composites, J. Energy Storage 105 (2025) 114612.
[9] A.M. Elshaer, A.M.A. Soliman, M. Kassab, S. Mori, A.A. Hawwash, Experimental investigations on copper foam/PCM composite-based thermal control hardware (TCH) using foam samples with different pore sizes under intermittent thermal conditions, J. Energy Storage 72 (2023) 108320.
[10] L. Jiang, L. Zhao, R. Zhang, W. Zhang, X. Ma, Z. Niu, G. Chen, M. Li, Research of the thermal storage properties of thermally conductive carbon fiber-reinforced paraffin/olefin block copolymer composite phase change materials with thermotropic flexibility, J. Energy Storage 76 (2024) 109761.
[11] J. Hu, Z. Yao, A. Chen, C. Xiao, G. Zhang, X. Yang, High thermal-conductive phase change material by carbon fiber orientation for thermal management and energy conversion application, Appl. Therm. Eng. 265 (2025) 125566.
[12] M. Tahmasbi, M. Siavashi, A.R. Karimi, R. Tousi, A.H. Keshtkaran, The effects of fins number, metal foam, and helical coil on the thermal storage enhancement of the phase change material: An experimental study, Appl. Therm. Eng. 253 (2024) 123780, https://doi.org/10.1016/j.applthermaleng.2024.123780.
[13] S.A. Shaik, P.K. Nigam, S.K. Gugulothu, Advanced fin designs for improved thermal management in PCM-based latent heat storage systems, Appl. Therm. Eng. 272 (2025) 126337, https://doi.org/10.1016/j.applthermaleng.2025.126337.
[14] R. Kalbasi, M. Afrand, J. Alsarraf, M.-D. Tran, Studies on optimum fins number in PCM-based heat sinks, Energy 171 (2019) 1088–1099, https://doi.org/10.1016/j.energy.2019.01.070.
[15] B. Kok, Examining effects of special heat transfer fins designed for the melting process of PCM and Nano-PCM, Appl. Therm. Eng. 170 (2020) 114989.
[16] P. Lamberg, K. Siren, Analytical model for melting in a semi-infinite PCM storage with an internal fin, Heat Mass Transf. 39 (2003) 167–176.
[17] B. Kamkari, H. Shokouhmand, Experimental investigation of phase change material melting in rectangular enclosures with horizontal partial fins, Int. J. Heat Mass Transf. 78 (2014) 839–851, https://doi.org/10.1016/j.ijheatmasstransfer.2014.07.056.
[18] A. Sciacovelli, F. Gagliardi, V. Verda, Maximization of performance of a PCM latent heat storage system with innovative fins, Appl. Energy 137 (2015) 707–715.
[19] X.Y. Zhang, Y.T. Ge, P.Y. Lang, Experimental investigation and CFD modelling analysis of finned-tube PCM heat exchanger for space heating, Appl. Therm. Eng. 244 (2024) 122731.
[20] Z. Khan, Z.A. Khan, An experimental investigation of discharge/solidification cycle of paraffin in novel shell and tube with longitudinal fins based latent heat storage system, Energy Convers. Manag. 154 (2017) 157–167.
[21] C. Zhao, J. Wang, Y. Sun, S. He, K. Hooman, Fin design optimization to enhance PCM melting rate inside a rectangular enclosure, Appl. Energy 321 (2022) 119368.

[22] M. Gürtürk, B. Kok, A new approach in the design of heat transfer fin for melting and solidification of PCM, Int. J. Heat Mass Transf. 153 (2020) 119671.
[23] C. Ji, Z. Qin, Z. Low, S. Dubey, F.H. Choo, F. Duan, Non-uniform heat transfer suppression to enhance PCM melting by angled fins, Appl. Therm. Eng. 129 (2018) 269–279.
[24] W. Hua, X. Xu, X. Zhang, H. Yan, J. Zhang, Progress in corrosion and anti-corrosion measures of phase change materials in thermal storage and management systems, J. Energy Storage 56 (2022) 105883.
[25] O.M. Adesusi, O.R. Adetunji, S.I. Kuye, A.I. Musa, T.J. Erinle, O.B. Gbadamosi-Olatunde, S.O. Ipadeola, A comprehensive review of the materials degradation phenomena in solid-liquid phase change materials for thermal energy storage, Int. J. Thermofluids 18 (2023) 100360.
[26] G. Ferrer, A. Solé, C. Barreneche, I. Martorell, L.F. Cabeza, Corrosion of metal containers for use in PCM energy storage, Renew, Energy 76 (2015) 465–469.
[27] A. Vasu, F.Y. Hagos, M.M. Noor, R. Mamat, W.H. Azmi, A.A. Abdullah, T. K. Ibrahim, Corrosion effect of phase change materials in solar thermal energy storage application, Renew. Sust. Energ. Rev. 76 (2017) 19–33.
[28] F. Jafari, G. Semprini, A. Bonoli, Evaluating the impact of recycled ceramic-PCM compound and absorber tube positioning on the efficiency of flat-plate solar collector, Appl. Therm. Eng. 127189 (2025).
[29] P. Jaffar Abass, S. Muthulingam, Comprehensive assessment of PCM integrated roof for passive building design: a study in energo-economics, Energ. Build. 317 (2024) 114387, https://doi.org/10.1016/J.ENBUILD.2024.114387.
[30] S. Yang, Y. Zhang, Y. Zhao, J.F. Torres, X. Wang, PCM-based ceiling panels for passive cooling in buildings: a CFD modelling, Energ. Build. 285 (2023) 112898, https://doi.org/10.1016/J.ENBUILD.2023.112898.
[31] N. Madeswaran, F.J. Desai, E. Asmatulu, Life cycle inventory and performance analysis of phase change materials for thermal energy storages, Emerg. Mater. 4 (2021) 1697–1709.
[32] B. Nienborg, S. Gschwander, G. Munz, D. Fröhlich, T. Helling, R. Horn, H. Weinläder, F. Klinker, P. Schossig, Life Cycle Assessment of thermal energy storage materials and components, Energy Procedia 155 (2018) 111–120.
[33] Rubitherm Technologies GmbH, Techdata – RT44HC, Berlin, Germany. https://www.rubitherm.eu/en/productcategory/organische-pcm-rt, 2025 (accessed August 12, 2025).
[34] F. Jafari, G. Semprini, A. Bonoli, Evaluating thermal storage capability of recycled construction materials: an experimental approach, Mater Renew Sustain. Energy 14 (2025) 1–13.
[35] N. Bagdassarov, N. Bagdassarov, Fundamentals of rock physics, Cambridge University Press, 2021.
[36] F.G.A. Verheijen, A. Zhuravel, F.C. Silva, A. Amaro, M. Ben-Hur, J.J. Keizer, The influence of biochar particle size and concentration on bulk density and maximum water holding capacity of sandy vs sandy loam soil in a column experiment, Geoderma 347 (2019) 194–202.
[37] Y. Yan, L. Zhang, X. Luo, C. Li, F. Hu, A new method for calculating the primary porosity of unconsolidated sands based on packing texture: Application to modern beach sand, Mar. Pet. Geol. 98 (2018) 384–396.
[38] M. Gustavsson, N.S. Saxena, E. Karawacki, S.E. Gustafsson, Specific heat measurements with the hot disk thermal constants analyser, in: Thermal Conductivity 23, CRC Press, 2021, pp. 56–65.
[39] S.K. Haigh, Thermal conductivity of sands, Geotechnique 62 (2012) 617–625.
[40] A. Alrtimi, M. Rouainia, S. Haigh, Thermal conductivity of a sandy soil, Appl. Therm. Eng. 106 (2016) 551–560.
[41] T. Ruuska, J. Vinha, H. Kivioja, Measuring thermal conductivity and specific heat capacity values of inhomogeneous materials with a heat flow meter apparatus, J. Build. Eng. 9 (2017) 135–141.
[42] K. Liu, Z. Wang, C. Jin, F. Wang, X. Lu, An experimental study on thermal conductivity of iron ore sand cement mortar, Constr. Build. Mater. 101 (2015) 932–941.
[43] M. Koru, Determination of Thermal Conductivity of Closed-Cell Insulation Materials That Depend on Temperature and Density, Arab. J. Sci. Eng. 41 (2016) 4337–4346, https://doi.org/10.1007/S13369-016-2122-6/METRICS.
[44] Z.N. Meng, P. Zhang, Experimental and numerical investigation of a tube-in-tank latent thermal energy storage unit using composite PCM, Appl. Energy 190 (2017) 524–539.
[45] M. Fadl, P.C. Eames, An experimental investigation of the heat transfer and energy storage characteristics of a compact latent heat thermal energy storage system for domestic hot water applications, Energy 188 (2019) 116083.
[46] K. Tofani, S. Tiari, Nano-enhanced phase change materials in latent heat thermal energy storage systems: a review, Energies (Basel) 14 (2021) 3821.
[47] T. Ambreen, H. Niyas, P. Kanti, H.M. Ali, C.-W. Park, Experimental investigation on the performance of RT-44HC-nickel foam-based heat sinks for thermal management of electronic gadgets, Int. J. Heat Mass Transf. 188 (2022) 122591.
[48] M. Fadl, D. Mahon, P.C. Eames, Thermal performance analysis of compact thermal energy storage unit-An experimental study, Int. J. Heat Mass Transf. 173 (2021) 121262, https://doi.org/10.1016/J.IJHEATMASSTRANSFER.2021.121262.
[49] J.R. Taylor, Error analysis, in: Univ. Science Books, Sausalito, California 20, 1997.
[50] J. Jcgm, Evaluation of measurement data—Guide to the expression of uncertainty in measurement, Int. Organ. Stand. Geneva ISBN 50 (2008) 134.
[51] Z. Tan, X. Li, X. Huai, K. Cheng, J. Chen, Experimental study on flow boiling heat transfer characteristics of microencapsulated phase change material suspension, J. Therm. Sci. 32 (2023) 1547–1557.
[52] L. Lin, D. Yang, Z. Luo, D. Liu, S.P. Lohani, S. Jia, L. Zhu, Y. Zhao, H. Yang, Q. Xu, Y. Ding, Numerical study on melting and heat transfer characteristics of vertical cylindrical PCM with a focus on the solid-liquid interface heat transfer rate, J. Energy Storage 72 (2023) 108370, https://doi.org/10.1016/J.EST.2023.108370.
[53] K.A. Hammoodi, W.N. Abbas, A.H. Askar, M.A. Alomari, A.M. Hassan, H. Q. Hussein, A.F. Khalaf, M.A. Flayyih, S.A. Kadhim, CFD simulation of air layer effects on RT42 PCM melting in a square cell, Sci. Rep. 15 (2025) 1–14, https://doi.org/10.1038/S41598-025-16573-6;SUBJMETA.